S-Shaped *I–V* Characteristics of Organic Solar Cells: Solving Mazhari's Lumped-Parameter Equivalent Circuit Model

Beatriz Romero, Gonzalo del Pozo, Belén Arredondo, Diego Martín-Martín, María P. Ruiz Gordoa, Andrew Pickering, Ana Pérez-Rodríguez, Esther Barrena, and Francisco J. García-Sánchez, *Senior Member, IEEE*

Abstract— We explain how to obtain closed-form analytic solutions from the set of equations that describe the three-diode lumped-parameter equivalent circuit model proposed by Mazhari [1] to portray the undesirable S-shape often observed in *I–V* characteristics of illuminated organic solar cells (OSCs), and occasionally seen in other types of solar cells. This allows quick extraction of the model's parameter values by directly fitting the resulting closed-form solution to the cell's measured *I–V* data. Such mathematical simplification of the extraction procedure facilitates individually studying the effect of each parameter on the illuminated OSC *I–V* characteristics, and thus on its power generation capacity. We illustrate application of the direct extraction procedure to measured *I–V* characteristics of an experimental OSC, which exhibits the illumination intensity-dependent S-shapes. The usefulness of the analytic solution to assess the effect of the model parameters is further corroborated by graphically illustrating the progression of a series of hypothetical synthetic *I–V* characteristics generated by this analytic solution using gradually changing the parameter values. Analysis of the results, in this case, indicates that activation of the diode that represents recombination is the key factor responsible for the emergence of the illuminated *I–V* curve's S-shape.

Index Terms— Organic solar cell (OSC) equivalent circuit model, S-shaped anomaly, S-shaped kink, S-shaped *I–V* characteristics.

I. INTRODUCTION

ORGANIC photovoltaics offer some advantages over traditional silicon-based solar cells, such as low cost and low environmental impact production, lightweight, thin, flexible, and semitransparent devices [2]. Among all available organic solar cell (OSC) structures, the concept of bulk-heterojunction has become popular because of its manufacturing ease coupled to the possibility of achieving relatively high efficiencies [3], [4].

One important issue often encountered in OSCs is the so-called S-shaped deformation, or kink, that sometimes emerges near the open-circuit voltage point in the $I-V$ curves measured under illumination. This detrimental effect lowers the curve's fill factor that results in reduced conversion efficiency [5]–[7]. This kink's origin has been attributed in OSCs to various physical phenomena: charge accumulation at the cathode interface [8], [9], presence of strong interface dipoles [10], unbalanced charge transport, and interfacial energy barriers. S-shaped $I-V$ curves have been observed in the cells of different materials and structures [11]–[13], as well as in inorganic solar cells, such as PbS quantum dots [14], CdTe [15], [16], III–V tandems [17], and graphene-silicon Schottky barrier solar cells [18].

Equivalent circuit modeling allows simulation, analysis, and optimization of device performance. Standard single-diode lumped-parameter equivalent circuit models commonly used for inorganic solar cells are also used for organic photovoltaic devices [19], [20]. However, such simple models are unable to reproduce by themselves, the possible presence of the mentioned S-shaped deformation in the $I-V$ characteristics. Thus, the other models and modifications have been proposed to specifically account for this undesirable feature.

A two-diode model was originally proposed by de Castro *et al.* [8]. Its describing equation was later analytically solved using the Lambert-W function [21], [22]. That model may be seen as a simplified version of the circuit shown

This article has been accepted for inclusion in a future issue of this journal. Content is final as presented, with the exception of pagination.

2   IEEE TRANSACTIONS ON ELECTRON DEVICES
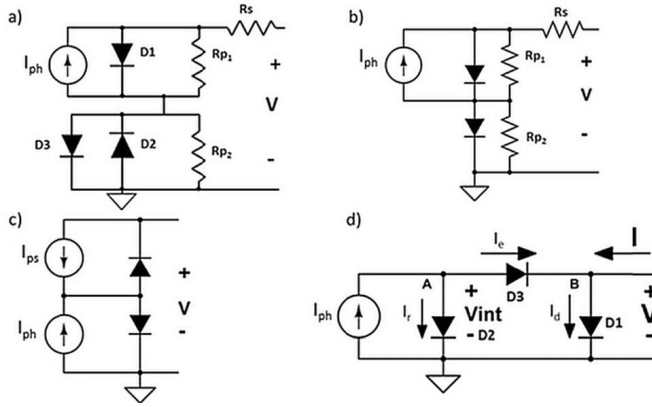

Fig. 1. Lumped-parameter equivalent circuits that have been proposed to model S-shaped $I–V$ characteristics, by (a) F. Castro *et al.* [22], (b) Zhuo *et al.* [23], (c) Gao *et al.* [14], and (d) Mazhari [1].

in Fig. 1(a) (with D3 open circuited). It includes a reverse bias-connected diode D2, which together with an additional shunt resistance R_{p2} is responsible for producing the S-shaped kink. This two-diode circuit has been used to model both OSC [8] and CdTe solar cells [15]. Zhuo *et al.* [23] have proposed another two-diode model, shown in Fig. 1(b), in which an additional subcircuit, made up of the parallel combination of forward bias diode D2 and R_{p2} is connected in series with the standard single-diode equivalent circuit model. This added subcircuit is responsible for creating the S-shaped kink, since its purpose is to model the Schottky junction at the anode and donor layer interface. Gao *et al.* [14] proposed a two-diode circuit model, shown in Fig. 1(c), with a diode D2 parallel connected to a photogenerated current source to produce the roll over observed in the $I–V$ characteristics of quantum dot solar cells.

A third diode must be included in the equivalent circuit model in order to reproduce the distinct additional current upturn that at times is visible beyond the S-shaped kink. Some three-diode circuits have been proposed to that effect. They are: 1) García-Sánchez *et al.* [24] proposed a variant of the original two-diode de Castro *et al.* [8] circuit, replacing R_{p2} by a third forward-biased diode D3 connected in parallel with the second reverse-biased diode D2, a circuit similar to that shown in Fig. 1(a) but without R_{p2} (R_{p2} is open circuited); 2) de Castro *et al.* [22] proposed the same three diode equivalent circuit model but restoring R_{p2}, now connected in parallel with both D2 and D3, as shown in the complete circuit of Fig. 1(a); and 3) a very different three-diode equivalent circuit, shown in Fig. 1(d), was proposed by Mazhari [1] to model the photovoltaic characteristics of OSC in the absence of significant parasitic series and shunt resistances.

Mazhari's model, which is the subject of this paper, assumes that the photogenerated current does not remain constant from short- to open-circuit conditions. The equivalent circuit, as shown in Fig. 1(d), includes a first diode D1, to model the dark current (majority carrier recombination); a second diode D2, to account for polaron recombination, a process that is light dependent; and a third diode D3, to model the extraction of free carriers. The two additional diodes,

D2 and D3 are connected in such a manner that they operate in forward condition only under illumination [see Fig. 1(d)] and are reverse-biased when the cell is not illuminated, and thus they have no impact on the dark $I–V$ characteristics. The D2 recombination diode is responsible for producing the S-shaped kink, since it decreases the extraction current.

Mazhari's model is the simplest among the three-diode models regarding parameters involved. It has only seven (three reverse saturation currents, three ideality factors, and the photogenerated current I_{ph}), as compared to eight in the García-Sanchez *et al.* [24] model, or nine in the complete de Castro *et al.* [22] model.

Since it is not mathematically possible to obtain a general analytical expression relating the terminal current and voltage, Mazhari [1] solved a simplified version of his model shown in Fig. 1(d) substituting D2 and D3 by resistances to simplify tedious numerical calculations.

However, there are cases where closed-form analytic solutions are possible without resorting to approximations depending on the ratio between the ideality factors of the extraction and recombination diodes, as m/n, where m and n are the integer's ≤ 4.

The fundamental novelty of this paper is the use, for the first time as far as we know, of an analytical closed-form mathematical expression to easily extract and promptly analyze the parameters of Mazhari's equivalent circuit model.

The immediate contribution is to avoid the need for iterative numerical solutions to express the OSC terminal variables. This way the equivalent circuit model may be readily used to simulate the S-shaped $I–V$ characteristics of illuminated OSCs. This is significant because, although numerical solutions might not be particularly difficult, they are notoriously cumbersome, time consuming, and are prone to conceal functional meaning. The proposed analytical expression helps to significantly speed up the process of fitting the model to measured $I–V$ data to extract the models' parameter values. The analytic closed-form permits to better visualize the effect of each model parameter on the overall shape of the $I–V$ characteristics, thus facilitating the study of underlying physical phenomena.

II. MODEL'S EQUATION SOLUTION

Fig. 1(d) shows the lumped-parameter equivalent circuit, without series and shunt resistive losses, proposed by Mazhari [1] to model S-shaped $I–V$ characteristics of OSCs. As already mentioned, this model includes two additional diodes in the standard one-diode model: A diode D2 to represent the loss of polarons due to recombination, and a diode D3 to characterize the extraction of free carriers. Application of Kirchhoff's current law to the circuit of Fig. 1(d), yields

$$I = I_d - I_e \tag{1}$$

$$I_{ph} = I_e + I_r = I_d - I + I_r \tag{2}$$

where I is the total current flowing through the circuit, I_{ph} is the photogenerated current, and I_d, I_e, and I_r are the dark, extraction, and recombination currents, respectively. Substituting the standard diode $I–V$ equations into (1), we can

This article has been accepted for inclusion in a future issue of this journal. Content is final as presented, with the exception of pagination.

ROMERO *et al.*: S-SHAPED *I–V* CHARACTERISTICS OF OSCs

3

express V_{int} (the voltage drop across the recombination diode) as a function of V as follows:

$$I = I_{d0}(e^{\alpha_d V} - 1) - I_{e0}\left[e^{\alpha_e(V - V_{\text{int}})} - 1\right]$$

$$\Rightarrow e^{\alpha_e V_{\text{int}}} = \left[I_{e0} + I_{d0}(e^{\alpha_d V} - 1) - I\right]\frac{e^{\alpha_e V}}{I_{e0}} \qquad (3)$$

where I_{d0} and I_{e0} are the reverse saturation currents of the dark and extraction diodes, respectively, and α_d and α_e are the parameters defined as $\alpha = q/(\eta k_B T)$, where η is the diode, ideality factor, k_B is the Boltzmann's constant and T is absolute temperature.

From (2) and (3) the photogenerated current is

$$\begin{aligned}
I_{\text{ph}} &= I_{d0}e^{\alpha_d V} - I_{d0} - I - I_{r0} + I_{r0}e^{\alpha_e V_{\text{int}}}\\
&= I_{d0}e^{\alpha_d V} - I_{d0} - I - I_{r0}\\
&\quad + I_{r0}\left\{\left[I_{e0} + I_{d0}(e^{\alpha_d V} - 1) - I\right]\frac{e^{\alpha_e V}}{I_{e0}}\right\}^{\frac{\alpha_r}{\alpha_e}} \qquad (4)
\end{aligned}$$

where I_{r0} is the reverse saturation current of the recombination diode and α_r is the parameter related to the ideality factor η_r.

Using the change of variable

$$Y = I_{e0} + I_{d0}(e^{\alpha_d V} - 1) - I \qquad (5)$$

the photogenerated current in (4) can be rewritten as

$$\begin{aligned}
I_{\text{ph}} &= Y - I_{e0} - I_{r0} + I_{r0}\left(\frac{Y e^{\alpha_e V}}{I_{e0}}\right)^{\frac{\alpha_r}{\alpha_e}}\\
&= Y - I_{e0} - I_{r0} + \frac{I_{r0}}{I_{e0}^{\alpha_r/\alpha_e}}e^{\alpha_r V}Y^{\alpha_r/\alpha_e}. \qquad (6)
\end{aligned}$$

Assuming that α_r/α_e is a rational number, i.e., $\alpha_r/\alpha_e = m/n$, and using the following change variable:

$$Y = Z^n. \qquad (7)$$

Equation (6) simplifies to

$$I_{\text{ph}} = -I_{e0} - I_{r0} + Z^n + \frac{I_{r0}e^{\alpha_r V}}{I_{e0}^{\alpha_r/\alpha_e}}Z^m. \qquad (8)$$

Finally, collecting terms by letting $A = I_{r0}e^{\alpha_r V}/I_{e0}^{\alpha_r/\alpha_e}$ and $B = I_{\text{ph}} + I_{e0} + I_{r0}$, (8) becomes

$$Z^n + AZ^m = B. \qquad (9)$$

Equation (9) is a polynomial in Z of degree equal to max $[m$ and $n]$ that can be numerically solved in general for any values of m and n. In general, for any values of the ideality factors, it is possible to define an irreducible ratio $n/m = \alpha_r/\alpha_e$. Then, a given n/m represents an infinite number of possibilities for the values of α_r and α_e.

The polynomial indicated by (9) can be analytically solved for Z under certain circumstances, specifically when the values of m and n are ≤ 4. We show below analytical solutions of (9) for three illustrative cases, so that the reader may appreciate the functional form. For $m = 1$ and $n = 1$, the current is given by

$$\begin{aligned}
I = I_{e0} + I_{d0}\left(e^{\alpha_d V} - 1\right)\\
- (I_{\text{ph}} + I_{e0} + I_{r0})\Big/\left(1 + \frac{I_{r0}e^{\alpha_r V}}{I_{e0}e^{\alpha_r/\alpha_e}}\right). \qquad (10)
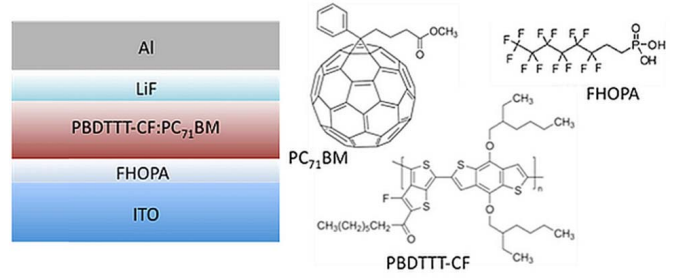\end{aligned}$$

Fig. 2. Layer structure of the devices (left) and chemical structure of the materials used for the active layer and hole transport layer (right).

For $n = 2$ and $m = 1$, the current is given by

$$\begin{aligned}
I = I_{e0} + I_{d0}(e^{\alpha_d V} - 1) - \frac{1}{2}\left(\frac{I_{r0}e^{\alpha_r V}}{I_{e0}e^{\alpha_r/\alpha_e}}\right)^2 - I_{\text{ph}} - I_{r0}\\
- I_{e0} \pm \frac{I_{r0}e^{\alpha_r V}}{I_{e0}e^{\alpha_r/\alpha_e}}\sqrt{\frac{1}{4}\left(\frac{I_{r0}e^{\alpha_r V}}{I_{e0}e^{\alpha_r/\alpha_e}}\right)^2 + I_{\text{ph}} + I_{e0} + I_{r0}}.
\end{aligned}$$
$$\qquad (11)$$

For $n = 1$ and $m = 2$, the current is given by

$$\begin{aligned}
I = I_{e0} + I_{d0}(e^{\alpha_d V} - 1) + \frac{1}{2}\frac{I_{e0}e^{\alpha_r/\alpha_e}}{I_{r0}e^{\alpha_r V}}\\
\mp \sqrt{\frac{1}{4}\left(\frac{I_{e0}e^{\alpha_r/\alpha_e}}{I_{r0}e^{\alpha_r V}}\right)^2 + (I_{\text{ph}} + I_{e0} + I_{r0})\frac{I_{e0}e^{\alpha_r/\alpha_e}}{I_{r0}e^{\alpha_r V}}}. \qquad (12)
\end{aligned}$$

Higher values of m or n, up to four (i.e., 1/3, 3, 2/3, 3/2, and 1/4, 4...) reproduce more complex functional forms of I which may be obtained using known solutions of third and fourth degree polynomials. Ratios outside the $1/4 \leq m/n \leq 4$ range are not of practical interest because they do not describe S-shaped kinks inside the fourth quadrant, as will be explained in Section IV.

The significance of the proposed solution is not meaningfully reduced in practice by its validity limitations because its applicability covers a wide range of possibilities. We wish to recall that in real practical devices when an S-shape comes into view, it usually shows up in the power producing fourth quadrant [5], [7]–[10]. Therefore, this range of α_r/α_e from 0.25 to 4 is clearly enough to describe all cases of any practical interest. Once the polynomial (9) is analytically solved for Z, the variable changes (7) and (5) are reverted and a closed-form analytical expression of the terminal current is obtained.

III. VALIDATION

The model's solution was validated using measured $I–V$ data of an experimental OSC based on poly [4,8-bis-substituted-benzo [1, 2-b:4, 5-b0] dithiophene-2, 6-diyl-alt-4-substituted ---thieno [3, 4-b] thio- phene-2, 6-diyl] derivative (PBDTTT-CF) and phenyl-C71-butyric-acid-methyl Ester (PC71BM). Devices use 3, 3, 4, 4, 5, 5, 6, 6, 7, 7, 8, 8, 8-tridecafluorooctyl phosphonic acid, and a self-assembled monolayer (SAM) as interlayer deposited onto ITO, instead of the widely employed PEDOT: PSS. SAMs are known to stabilize and modify ITOs workfuncion [25].

The layer structure is shown in Fig. 2. The cell's area is 0.105 cm^2. $I–V$ characteristics used for the model validation

This article has been accepted for inclusion in a future issue of this journal. Content is final as presented, with the exception of pagination.

4   IEEE TRANSACTIONS ON ELECTRON DEVICES
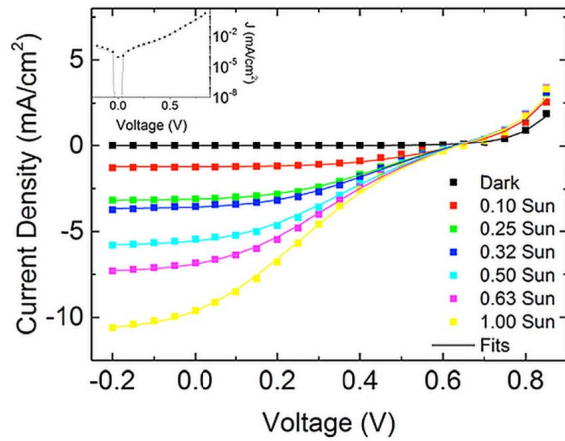

Fig. 3. I–V characteristics of the experimental OSC described in Section III, at different illumination intensities, showing the measured data (symbols) and the model playbacks calculated using Mazhari's model analytical solution (solid lines). Inset shows the dark characteristic in a semilog scale.

Fig. 4. (a) Reverse saturation current and (b) photogenerated current as functions of illumination intensity.

were recorded under dark and under AM 1.5 solar spectrum illumination conditions at intensities varying from 0.1 to 1 sun. The I–V curves used here belong to one of the devices of a batch of 48 samples, with four devices per sample, all of which exhibited highly reproducible results.

The first step of the parameter extraction is to fit the standard one-diode solar cell model to the measured dark I–V curves to get the dark diode parameters. The values extracted from the best fit (see inset of Fig. 3) are: reverse saturation current $I_{d0} = 1.5 \times 10^{-8}$ A and ideality factor $\eta_d = 2.8$, which is higher than those of typical inorganic solar cells.

Although it is not uncommon to obtain high ideality factors when modeling I–V characteristics of OSCs with Shockley-type equations [26], it is best to exercise some caution and regard such high values only as apparent ideality factors that might or might not directly represent real physical phenomena.

The second step is to fit the analytical solution of the model to the illuminated I–V characteristics. Dark diode parameters were kept constant and equal to those obtained previously.

After many fits using different approaches, we concluded that the S-shape does not strongly depend on the parameters associated with the extraction diode. Rather, the S-shape is mainly determined by I_{r0}.

According to this, and in order to reduce the number of free parameters I_{e0}, η_e, and η_r were fixed to a value that minimized the error. On the other hand, I_{r0} and I_{ph} are left free to vary with illumination level. The fitting procedures were carried out for values of m and $n = 1, 2, 3,$ and 4 yielding the following ideality factor ratios $\alpha_r/\alpha_e = 1, 1/2, 1/3, 1/4, 2, 2/3, 3, 3/2, 3/4,$ and $4/3$. The error function used was $\sum_i [y_i - f(x_i)]^2$, where y_i is the experimental current and $f(x_i)$ is the simulated current calculated at x_i (the experimental voltage). The smallest fitting error was obtained for $\alpha_r/\alpha_e = 2$ for all I–V curves simulated under various illumination levels.

Fig. 3 shows measured data (symbols) and the playback of the closed-form equation (solid lines) that describes Mazhari's model, using the extracted parameter values. Fig. 3 indicates
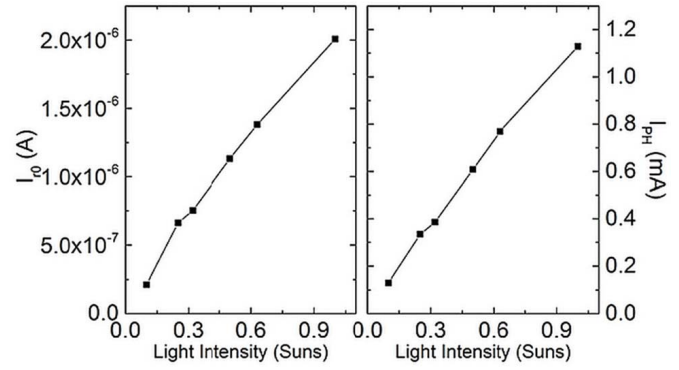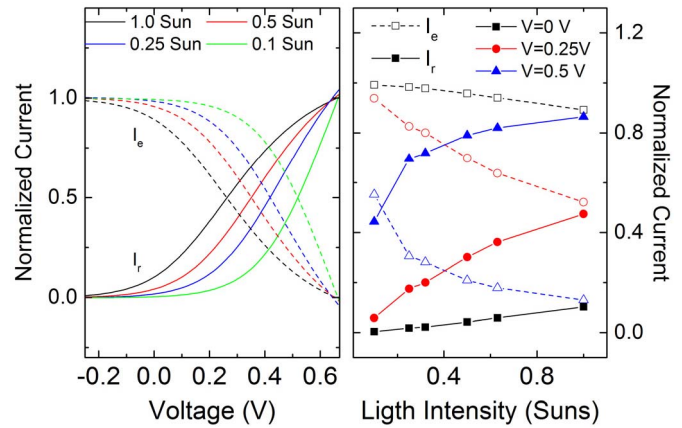

Fig. 5. (a) Normalized extraction and recombination currents versus voltage at different light intensities. (b). Normalized extraction and recombination currents versus light intensity at different voltages.

that there is a good agreement between experimental data and Mazhari's model analytical solution. The inset of Fig. 3 shows, in a semilogarithmic scale, the data (dots) and the fit solution (solid line) under dark conditions. Parameters obtained from the fitting procedure were $\eta_e = 8$, $\eta_r = 4$, and $I_{e0} = 1.44$ mA/cm^2.

Fig. 4(a) and (b) shows that the parameters I_{r0} and I_{ph} increase linearly with light intensity. Although this dependence of parameter I_{r0} might seem unexpected, the values extracted from this OSC I–V curves led to conclude that the value of I_{r0} increases with light intensity. Such result is in agreement with those obtained by Tress et al. [27] and [28]. As these authors suggest, an accumulation of photogenerated carriers at the donor / HTL interface partially screens the field, resulting in a high voltage drop at the HTL, while the field is reduced at the donor / acceptor interface. This lowered field results in higher recombination probability at the donor / acceptor interface, which traduces into an increase of recombination current I_{r0} with light intensity in Mazhari's model. The rise in voltage across the recombination diode (V_{int}) as I_{ph} increases is insufficient to accommodate such increment of I_{rec}, forcing I_{r0} to also rise with light intensity.

Fig. 5(a) shows the extraction current I_e and the recombination current I_r at different light intensities normalized to I_{ph}. At low voltages, extraction current reaches its maximum value

This article has been accepted for inclusion in a future issue of this journal. Content is final as presented, with the exception of pagination.

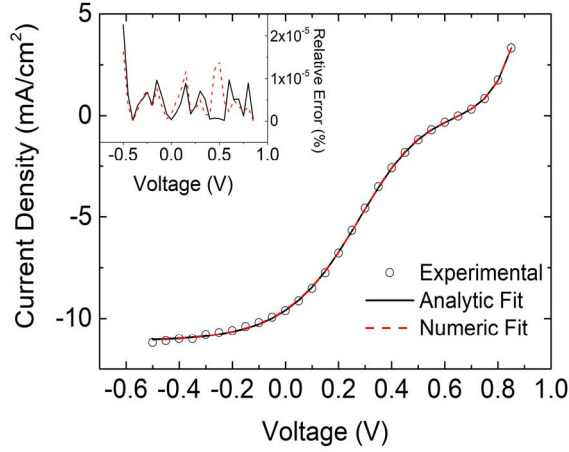ROMERO *et al.*: S-SHAPED *I–V* CHARACTERISTICS OF OSCs
5

Fig. 6. Experimental and simulated *I–V* characteristics at 1 sun using numerical and analytic versions of Mazhari's model. Inset shows relative error of analytical and numerical fits.

Fig. 7. Simulated $I - V$ characteristics with varying parameter values (a) I_{e0}, (b) I_{r0}, (c) η_e, and (d) η_r. Default values of parameters are $I_{e0} = 1 \times 10^{-3}$ A, $I_r0 = 1 \times 10^{-5}$ A, $\eta_e = 8$, $\eta_r = 4$, and $I_{ph} = 10$ mA.

and thus recombination current $I_e = 0$. In this condition no S-shaped kink is observed. On the other hand, at higher voltages, the recombination current I_r reaches its maximum and thus extraction becomes 0, resulting in a pronounced S-shaped kink. The voltage value at which the recombination and extraction currents become equal decreases with light intensity from 0.52 V (at 0.1 sun) to 0.25 V (at 1 sun). Thus, we conclude that as illumination increases, the S-shape shifts to lower voltages.

Fig. 5(b) shows recombination and extraction currents versus light intensity at different voltages (0, 0.25, and 0.5 V). At 0 V the extraction current dominates over the recombination current regardless of illumination level. At 0.5 V the recombination current dominates over the extraction current (except at 0.1 sun) causing the emergence of the S-shape. At 0.25 V the extraction current dominates over recombination current at low light intensities, and both currents tend to the same value at 1 sun.

The experimental characteristic measured at 1 sun was fit both numerically and analytically to compare both solutions. As Fig. 6 shows, both fits are practically identical. Their relative errors, shown in the inset, indicate that both approaches provide similar accuracy.

IV. EFFECTS OF INDIVIDUAL MODEL PARAMETERS

Several simulations were carried out using the analytic solution, proposed here, to study the influence of individual parameters of the equivalent circuit model on the overall S-shaped *I–V* characteristics. Synthetic *I–V* characteristics were calculated varying one parameter at a time. Inverse saturation currents were varied over several orders of magnitude, while the ideality factors were varied only within values that fulfill the condition n/m (for n and $m \leq 4$). Fig. 7 shows synthetic *I–V* characteristics for varying values of η_e, η_r, I_{e0}, and I_{r0}, while the other parameters remain constant. Default values used are: $I_{e0} = 1 \times 10^{-3}$ A, $I_{r0} = 1 \times 10^{-5}$ A, $\eta_e = 8$, $\eta_r = 4$, and $I_{ph} = 10$ mA. These results indicate that a decreasing η_e or increasing η_r shifts the S-shaped kink location toward higher voltage values. Similarly, an increasing I_{e0} or
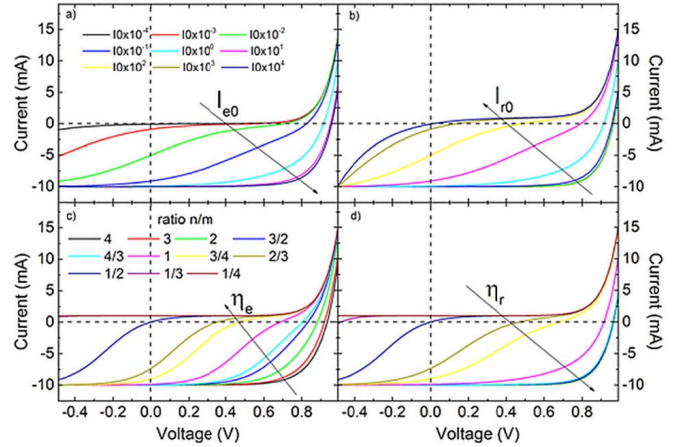
decreasing I_{r0} also shifts the location of the S-shaped kink toward higher voltage values.

A quick assessment confirms that, as expected, the S-shaped kink tends to vanish when recombination current decreases and becomes negligible compared to the extraction current. This can be achieved by either increasing η_r or decreasing I_{r0}.

Fig. 7(c) and (d) shows that ratios of m/n beyond four (recombination dominating over extraction) move the S-shaped kink well into the third quadrant. On the other hand, ratios below 0.25 (extraction dominating over recombination) cause the S-shape to vanish.

V. COMPARISON WITH OTHER LUMPED-CIRCUIT MODELS

The use of the presently proposed analytic solution of Mazhari's equivalent-circuit model's equation, allows to easily simulate the synthetic S-shaped *I–V* characteristics for phenomenological analysis. We have compared different lumped-equivalent circuits used to model S-shaped kinks in the illuminated *I–V* characteristics. An *I–V* characteristics of the experimental OSC measured at 1 sun illumination intensity (the curve that exhibits a more pronounced S-shape) was fit with: 1) Mazhari's model; 2) de Castro *et al.* [8] two-diode model; and 3) de Castro *et al.* [22] three diode model]. In the last two models R_s was set to zero in order to reduce the number of fitting parameters. The fitting procedure was performed within the voltage range from -0.2 to 0.85 V. The first two models have seven fitting parameters while the last one has nine parameters. The fitting errors obtained are 2.8×10^{-10}, 7×10^{-10}, and 8.5×10^{-13}, respectively. The time elapsed to carry out fitting was 117, 126, and 190 s, respectively, using a laptop computer equipped with a fourth-generation Intel Core i7-4710HQ processor. Based on these results, it appears that Mazhari's model produces only a slightly better fit than the original de Castro *et al.* [8] model, with very similar computational times. The tree-diode de Castro *et al.* [22] model produces three orders of magnitude lower errors, but requires two extra parameters, and the computational time is slightly higher.

This article has been accepted for inclusion in a future issue of this journal. Content is final as presented, with the exception of pagination.

6   IEEE TRANSACTIONS ON ELECTRON DEVICES

VI. CONCLUSION

We have established that Mazhari's three-diode lumped-parameter equivalent circuit model for S-shaped solar cell $I-V$ characteristics has exact analytic solutions for several practical cases, when the ratio between extraction and recombination ideality factors is m/n with m and $n \leq 4$.

We extracted Mazhari's model parameters by directly fitting the presently proposed analytic solution to the $I-V$ data of an experimental PBDTTT-CF:PC$_{71}$BM-based OSC measured at various illumination levels from dark to 1 sun. Results show that as light intensity increases, the location of the S-shaped kink moves to lower voltage values due to the increase of the recombination current. Significant computational time reduction over otherwise tedious numerical calculations is achieved by using the analytic solution. Using trial synthetic $I-V$ characteristics generated with this analytical solution, we were able to easily establish by independently varying each model parameter, that the S-shaped kink tends to vanish when the free charge extraction mechanism significantly dominates over the polaron recombination phenomenon.

We finally compared Mazhari's three-diode lumped-equivalent circuit model to other two equivalent circuits that are also used to model S-shaped $I-V$ curves.

REFERENCES

[1] B. Mazhari, "An improved solar cell circuit model for organic solar cells," *Solar Energy Mater. Solar Cells*, vol. 90, no. 7, pp. 1021–1033, 2006, doi: 10.1016/j.solmat.2005.05.017.

[2] T. Kim *et al.*, "Flexible, highly efficient all-polymer solar cells," *Nature Coomun.*, vol. 6, Oct. 2015, Art. no. 8547, doi: 10.1038/ncomms9547.

[3] Z. He, C. Zhong, S. Su, M. Xu, H. Wu, and Y. Cao, "Enhanced power-conversion efficiency in polymer solar cells using an inverted device structure," *Nature Photon.*, vol. 6, no. 9, pp. 591–595, 2012, doi: 10.1038/nphoton.2012.190.

[4] Y. Liu *et al.*, "Aggregation and morphology control enables multiple cases of high-efficiency polymer solar cells," *Nature Commun.*, vol. 5, Nov. 2014, Art. no. 5293, doi: 10.1038/ncomms6293.

[5] A. Wagenpfahl, D. Rauh, M. Binder, C. Deibel, and V. Dyakonov, "S-shaped current-voltage characteristics of organic solar devices," *Phys. Rev. B, Condens. Matter*, vol. 82, no. 11, pp. 115306-1–115306-8, 2010, doi: 10.1103/PhysRevB.82.115306.

[6] A. Kumar, S. Sista, and Y. Yang, "Dipole induced anomalous S-shape $I-V$ curves in polymer solar cells," *J. Appl. Phys.*, vol. 105, no. 9, p. 094512, 2009, doi: 10.1063/1.3117513.

[7] B. Qi and J. Wang, "Fill factor in organic solar cells," *Phys. Chem. Chem. Phys.*, vol. 15, no. 23, pp. 8972–8982, 2013, doi: 10.1039/C3CP51383A.

[8] F. de Castro, J. Heier, F. Nüesch, and R. Hany, "Origin of the kink in current-density versus voltage curves and efficiency enhancement of polymer-C$_{60}$ heterojunction solar cells," *IEEE J. Sel. Topics Quantum Electron.*, vol. 16, no. 6, pp. 1690–1699, Nov./Dec. 2010, doi: 10.1109/JSTQE.2010.2040807.

[9] B. Ecker, H. J. Egelhaaf, R. Steim, J. Parisi, and E. von Hauff, "Understanding S-shaped current–voltage characteristics in organic solar cells containing a TiO$_x$ interlayer with impedance spectroscopy and equivalent circuit analysis," *J. Phys. Chem C*, vol. 116, no. 31, pp. 16333–16337, 2012, doi: 10.1021/jp305206d.

[10] M. Glatthaara *et al.*, "Efficiency limiting factors of organic bulk heterojunction solar cells identified by electrical impedance spectroscopy," *Solar Energy Mater. Solar Cells*, vol. 91, no. 5, pp. 390–393, 2007, doi: 10.1016/j.solmat.2006.10.020.

[11] D. Gupta, M. Bag, and K. S. Narayan, "Correlating reduced fill factor in polymer solar cells to contact effects," *Appl. Phys. Lett.*, vol. 92, no. 9, p. 093301, 2008, doi: 10.1063/1.2841062.

[12] M. R. Lilliedal, A. J. Medford, M. V. Madsen, K. Norrman, and F. C. Krebs, "The effect of post-processing treatments on inflection points in current–voltage curves of roll-to-roll processed polymer photovoltaics," *Solar Energy Mater. Solar Cells*, vol. 94, no. 12, pp. 2018–2031, 2010, doi: 10.1016/j.solmat.2010.06.007.

[13] W. Tress, A. Petrich, M. Hummert, M. Hein, K. Leo, and M. Riede, "Imbalanced mobilities causing S-shaped $I-V$ curves in planar heterojunction organic solar cells," *Appl. Phys. Lett.*, vol. 98, no. 6, p. 063301, 2011, doi: 10.1063/1.3553764.

[14] J. Gao, J. M. Luther, O. E. Semonin, R. J. Ellingson, A. J. Nozik, and M. C. Beard, "Quantum dot size dependent $J-V$ characteristics in heterojunction ZnO/PbS quantum dot solar cells," *Nanoletters*, vol. 11, no. 3, pp. 1002–1008, 2011, doi: 10.1021/nl103814g.

[15] S. H. Demtsu and J. R. Sites, "Effect of back-contact barrier on thin-film CdTe solar cells," *Thin Solid Films*, vol. 510, no. 1, pp. 320–324, 2006, doi: 10.1016/j.tsf.2006.01.004.

[16] A. Niemegeers and M. Gurgelman, "Effects of the Au/CdTe back contact on IV and CV characteristics of Au/CdTe/CdS/TCO solar cells," *J. Appl. Phys.*, vol. 81, no. 6, pp. 2881–2886, 1997, doi: 10.1063/1.363946.

[17] E. Veinberg-Vidal *et al.*, "Manufacturing and characterization of III–V on silicon multijunction solar cells," *Energy Procedia*, vol. 92, pp. 242–247, Aug. 2016, doi: 10.1016/j.egypro.2016.07.066.

[18] Y. Song *et al.*, "Role of interfacial oxide in high-efficiency graphene–silicon Schottky barrier solar cells," *Nano Lett.*, vol. 15, no. 3, pp. 2104–2110, 2015, doi: 10.1021/nl505011f.

[19] A. Jain and A. Kapoor, "A new approach to study organic solar cell using Lambert W-function," *Solar Energy Mater. Solar Cells*, vol. 86, no. 2, pp. 197–205, 2005, doi: 10.1016/j.solmat.2004.07.004.

[20] A. Cheknane, H. S. Hilal, F. Djeffal, B. Benyounce, and J.-P. Charles, "An equivalent circuit approach to organic solar cell modelling," *Microelectron. J.*, vol. 39, no. 10, pp. 1173–1180, 2008, doi: 10.1016/j.mejo.2008.01.053.

[21] B. Romero, G. D. Pozo, and B. Arredondo, "Exact analytical solution of a two diode circuit model for organic solar cells showing S-shape using Lambert W-functions," *Solar Energy*, vol. 86, no. 10, pp. 3026–3029, 2012, doi: 10.1016/j.solener.2012.07.010.

[22] F. de Castro, A. Laudani, F. Riganti, and A. Salvini, "An in-depth analysis of the modelling of organic solar cells using multiple-diode circuits," *Solar Energy*, vol. 135, pp. 590–597, Oct. 2016, doi: 10.1016/j.solener.2016.06.033.

[23] L. Zuo, J. Yao, H. Li, and H. Chen, "Assessing the origin of the S-shaped $I-V$ curve in organic solar cells: An improved equivalent circuit model," *Solar Energy Mater. Solar Cells*, vol. 122, pp. 88–93, Mar. 2014, doi: 10.1016/j.solmat.2013.11.018.

[24] F. J. García-Sánchez, D. Lugo-Muñoz, J. Muci, and A. Ortiz-Conde, "Lumped parameter modeling of organic solar cells' S-shaped $I-V$ characteristics," *IEEE J. Photovolt.*, vol. 3, no. 1, pp. 330–335, Jan. 2013, doi: 10.1109/JPHOTOV.2012.2219503.

[25] A. Sharma, B. Kippelen, P. J. Hotchkiss, and S. R. Marder, "Stabilization of the work function of indium tin oxide using organic surface modifiers in organic light-emitting diodes," *Appl. Phys. Lett.*, vol. 93, no. 16, p. 163308, 2008, doi: 10.1063/1.2998599.

[26] T. Kirchartz, F. Deledalle, P. S. Tuladhar, J. R. Durrant, and J. Nelson, "On the differences between dark and light ideality factor in polymer: Fullerene solar cells," *J. Phys. Chem. Lett.*, vol. 4, no. 14, pp. 2371–2376, 2013, doi: 10.1021/jz4012146.

[27] W. Tress and O. Inganäs, "Simple experimental test to distinguish extraction and injection barriers at the electrodes of (organic) solar cells with S-shaped current–voltage characteristics," *Solar Energy Mater. Solar Cells*, vol. 117, pp. 599–603, Oct. 2013, doi: 10.1016/j.solmat.2013.07.014.

[28] W. Tress, K. Leo, and M. Riede, "Influence of hole-transport layers and donor materials on open-circuit voltage and shape of $I-V$ curves of organic solar cells," *Adv. Funct. Mater.*, vol. 21, no. 11, pp. 2140–2149, 2011, doi: 10.1002/adfm.201002669.